Chloride binding and cholesterol effects on high frequency complex nonlinear capacitance (cNLC) in the mouse outer hair cell: experiment and molecular dynamics

Jun-Ping Bai [2], Chenou Zhang [5], Vijay Renigunta [6], Dominik Oliver [6], Dhasakumar Navaratnam [1,2,3], Oliver Beckstein [5], Joseph Santos-Sacchi [1,3,4]

[1]Surgery (Otolaryngology), [2]Neurology, [3]Neuroscience, and [4]Cellular and Molecular Physiology, Yale University School of Medicine, 333 Cedar Street, New Haven, CT 06510, USA

[5]Center for Biological Physics and Department of Physics, Arizona State University, Tempe, AZ 85287-1504 USA

[6]Institute for Physiology and Pathophysiology, Section of Neurophysiology, Philipps University Marburg, Deutschhausstr. 2, 35037 Marburg, Germany

Running title: high frequency prestin charge movements in the mouse

Keywords: capacitance, displacement currents, cochlea amplification, prestin, macro-patch, voltage-clamp, molecular dynamics

Send correspondence to:

Joseph Santos-Sacchi
Surgery (Otolaryngology), Neuroscience, and Cellular and Molecular Physiology
Yale University School of Medicine
BML 224, 333 Cedar Street
New Haven, CT 06510
Phone: (203) 785-7566
e-mail: joseph.santos-sacchi@yale.edu

Pages: 22
Figures: 6
Abstract: 338 words
Intro: 719 words
Discussion: 1047 words

Author contributions: J-PB performed patch experiments; JS-S performed and designed patch experiments, analyzed data, and wrote manuscript; CZ and OB performed, designed, analyzed MD simulations, and wrote portions of the manuscript; VR and DO supplied the KI mouse and edited manuscript; DN discussed experiments, simulations and edited manuscript.

Conflict of Interest: The authors declare no competing financial interests.

Acknowledgements: This research was supported by NIH-NIDCD R56DC021057, R01 DC016318 and R01 DC008130. Anton 2 computer time was provided by the Pittsburgh Supercomputing Center (PSC) under allocation MCB180088P through Grant R01GM116961 from the National Institutes of Health; the Anton 2 machine at PSC was generously made available by D.E. Shaw Research.

Abstract

The function of prestin (SLC26a5), an anion transport family member, has evolved to enhance auditory sensitivity and frequency selectivity by providing mechanical feedback via outer hair cells (OHC) into the organ of Corti. The frequency extent of this boost is governed by the voltage-dependent kinetics of the protein's charge movements, otherwise known as nonlinear capacitance (NLC) that we measure in membrane patches under voltage clamp. Here we extend our previous studies on guinea pig OHCs by studying the frequency response of NLC in the mouse OHC, a species with higher frequency auditory needs. We find that the characteristic frequency cut-off (F_{is}) for the mouse surpasses that of the guinea pig, being 27 kHz vs. 19 kHz, respectively; nevertheless, each shows significant activity in the ultrasonic range. We also evaluate the influence of anion binding on prestin frequency response. Several single point mutations within the chloride binding pocket of prestin (e.g., S396E, S398E) lack anion influence. In agreement, we show absence of anion binding through molecular dynamics (MD) simulations. NLC F_{is} in the S396E knock-in mouse remains the same as controls, indicating that high frequency activity is likely governed by viscoelastic loads within the membrane characterized by stretched-exponential frequency roll-off. Accordingly, treatment with MβCD, which removes membrane cholesterol, possibly from prestin itself, and can alter membrane fluidity, augments NLC F_{is} out to 39 kHz. Although interactions between membrane lipid and prestin have been suggested from structural studies to arise at their interfacial boundaries within the membrane, our MD simulations suggest that phospholipids can insert within transmembrane domains of prestin during voltage perturbation. Such novel lipid-protein interactions could account for our observed changes in the phase of prestin's voltage-sensor charge movements across frequency. We hypothesize that because prestin tertiary structures of all species studied to-date are indistinguishable, it is likely that any special auditory requirements of individual species for cochlear amplification have evolved to capitalize on prestin performance by modifying, not the protein itself, but the external loads on the protein, including those within the membrane and organ of Corti.

Significance

Prestin is believed to provide cochlear amplification in mammals that possess a wide range of frequency sensitivities, yet its tertiary structure is indistinguishable among those species studied. We find that prestin kinetics is faster in mice than in guinea pigs, mice showing higher frequency auditory capabilities. Chloride binding is not influential, but membrane lipids/viscosity is. We suggest that the evolution of prestin's species performance involves modifications of impinging loads, not the protein itself.

Introduction

The mammalian organ of Corti houses two types of sensory receptor cells, the inner (IHC) and outer hair cells (OHC). Each is responsive to sound stimuli, producing receptor potentials that are tuned to particular acoustic frequencies, depending upon the location of those cells along the tonotopic cochlear spiral (Russell and Sellick, 1978; Dallos et al., 1982). Unlike the IHC, the OHC additionally is mechanically active, producing changes in length when electrically stimulated (Brownell et al., 1985). That OHC mechanical activity, being voltage dependent (Santos-Sacchi and Dilger, 1988), is the basis of receptor potential-driven amplificatory feedback, termed cochlear amplification, that enhances auditory response sensitivity and selectivity of the IHC, the main sensory cell type. The voltage-dependent protein, prestin (Zheng et al., 2000), which resides exclusively in the OHC lateral membrane, underlies this process (Dallos et al., 2008). It is not surprising that chloride anions play a central role in OHC/prestin activity (Oliver et al., 2001; Santos-Sacchi et al., 2006a; Rybalchenko and Santos-Sacchi, 2008), since prestin (SLC26a5) is a member of the SLC26 anion transporter family (Geertsma and Oliver, 2023).

The mechanical activity of prestin arises from its voltage-sensor charge movement, traditionally measured as a robust nonlinear, bell-shaped, voltage-dependent capacitance (NLC) (Santos-Sacchi, 1991), which drives conformational switching of the protein. This activity across frequency is limited by the protein's kinetics within the plasma membrane (Santos-Sacchi and Tan, 2018). The characteristic speed of a voltage-dependent protein is identified at the membrane voltage (V_h) where sensor charge (Q) is equally distributed across the membrane field, namely, at the midpoint of its Q-V Boltzmann function or, correspondingly, at the peak of its NLC. Interestingly, prestin is also sensitive to membrane tension, shifting V_h and generating displacement currents upon membrane stretch, observations that have led to its characterization as piezoelectric-like (Iwasa, 1993; Gale and Ashmore, 1994; Kakehata and Santos-Sacchi, 1995; Takahashi and Santos-Sacchi, 2001; Santos-Sacchi and Tan, 2022). Though the frequency response of peak NLC under voltage clamp in guinea pig OHC membrane patches has a characteristic frequency roll-off near 10-20 kHz (Gale and Ashmore, 1997b; Dong et al., 2000; Santos-Sacchi and Tan, 2019; Santos-Sacchi and Tan, 2022), significant activity is measurable in the ultrasonic range (Santos-Sacchi et al., 2023)..

Recently, we found in guinea pig OHC patches that the frequency response of NLC can be augmented by increasing the fluidity of the plasma membrane with the general anesthetic chloroform (Santos-Sacchi and Tan, 2022), in line with previous indications that the lipid bilayer influences prestin

activity. For example, in addition to chloroform effects, the phospholipid HePC was shown to shift NLC V_h (Santos-Sacchi and Wu, 2004), and subsequent work has implicated other membrane lipids, including cholesterol (Rajagopalan et al., 2007; Sfondouris et al., 2008; Organ and Raphael, 2009; Fang et al., 2010). Indeed, cholesterol can influence prestin confinement/diffusion in the plasma membrane (Kamar et al., 2012). Furthermore, it has been argued that cryo-EM determined structures of prestin suggest an influential role of membrane lipids on prestin activity, even evidencing direct interactions with prestin (Bavi et al., 2021; Ge et al., 2021; Butan et al., 2022). Apart from lipids, we also find that chloride anions can influence prestin kinetics (Santos-Sacchi and Song, 2016; Santos-Sacchi and Tan, 2022), with mutations that affect anion binding site access having measurable effects (Takahashi et al., 2016; Takahashi et al., 2023). Since it is unlikely that prestin tertiary structure differs significantly among species, with gerbil, human and dolphin already determined (Bavi et al., 2021; Ge et al., 2021; Butan et al., 2022; Futamata et al., 2022), we have hypothesized that membrane lipid makeup or chloride concentration could vary along the cochlea spiral or among mammals to influence kinetics to match species-specific acoustic requirements (Santos-Sacchi and Tan, 2022). Here we extend our physiological studies to the mouse, a species with acoustic frequency sensation above that of the guinea pig, to investigate the influence of chloride binding and cholesterol on the high frequency kinetics of prestin. We utilize a prestin knock-in (KI) mouse (S396E), which lacks anion sensitivity, and use cyclodextrin (MβCD) to remove cholesterol. Additionally, we complement our investigations with molecular dynamics simulations. We find that lipids can influence high frequency NLC, but the ability to bind chloride does not. These data suggest that viscoelastic characteristics of the plasma membrane limit prestin's high frequency kinetics, not differences in any evolved prestin structure.

Materials and Methods

Nonlinear Capacitance

Control OHC complex NLC (cNLC) was measured in b6 mouse (Jackson Lab; 1-2 months old) macro-patches under voltage clamp, with current sampling at 1 MHz (16 bit NI-USB 6356; National Instruments) using an Axon 200B amplifier in capacitive feedback mode and Bessel filter set to 100 kHz. Analyses were made in jClamp (www.scisoftco.com) and Matlab (www.mathworks.com). Experimental methods for NLC assessment are fully detailed in (Santos-Sacchi et al., 2021; Santos-Sacchi et al., 2023). Briefly, extracellular solution was (in mM): NaCl 100, TEA-Cl 20, CsCl 20, $CoCl_2$ 2, $MgCl_2$ 1, $CaCl_2$ 1, Hepes 10, pH 7.2, and this solution was used in the on-cell patch pipette. Macro-patches were established on the OHC lateral plasma membrane, and swept-frequency AC voltage chirps (10 mV) were presented atop DC holding potentials ranging from +160 to -160 mV (see **Fig. 1** in (Santos-Sacchi et al., 2023)). The voltage chirps were generated

in jClamp using the Matlab logarithmic "chirp" function (10 mV pk; pts = 4096; F0 = 244.141 Hz; F1 = 500 kHz; t1 = 0.004095 s). Currents were corrected for system roll-off characteristics in the frequency domain. The methodology of Fernandez et al. (Fernandez et al., 1982) was used to extract real and imaginary components of cNLC from membrane admittance, $Y_m(\omega)$, as we previously described in detail (Santos-Sacchi et al., 2023). The complex components represent voltage sensor charge moving in phase (Im(cNLC)) and 90° out of phase (Re(cNLC)) with AC voltage, the former membrane-constrained charge movements being "resistive" and the latter being "capacitive" in nature. cNLC estimates were obtained following subtraction of linear admittance at +160 mV holding potential, where OHC NLC is absent, thereby removing stray capacitance effects. Currents were averaged 64 times, and spectra were obtained by FFT using 4096 data points. For recordings in whole cell mode, admittance analysis with 2-sine voltage ramps was performed as usual (Santos-Sacchi et al., 1998; Santos-Sacchi, 2004). MβCD (Sigma) in patch pipettes containing extracellular solutions ranged from 0.1 - 1 mM.

NLC was fit with a Boltzmann function (Santos-Sacchi, 1991; Santos-Sacchi and Navarrete, 2002).

$$C_m = NLC + C_{\text{lin}} = Q_{\text{max}} \frac{\text{ze}}{k_B T} \frac{b}{(1+b)^2} + C_{\text{lin}} \qquad eq.1$$

$$\text{where} \quad b = exp\left(-ze\frac{V_m - V_h}{k_B T}\right),$$

Q_{max} is the maximum nonlinear charge moved, V_h is voltage at peak capacitance or equivalently, at half-maximum charge transfer, V_m is membrane potential, z is valence, C_{lin} is linear membrane capacitance, e is electron charge, k_B is Boltzmann's constant, and T is absolute temperature. Experiments were performed at room temperature. Fits were made to real and imaginary components of **cNLC** across interrogation frequency. V_h for analyses was measured at 5.1 kHz. No junction potentials are expected for the symmetrical pipette/extracellular solutions. Average zero current voltages of the membrane patches, which correspond to cell potentials (Mason et al., 2005), were -0.72, -1.78 and +5.12 mV for the b6 control, MβCD treated, and S396E prestin OHCs, respectively, were used to correct V_h values.

As previously (Santos-Sacchi et al., 2023), we fit the Abs(cNLC) data with the Havriliak-Negami [HN] relaxation function (Alverez et al., 1991), the frequency domain representation of a stretched exponential function. Cut-off frequencies (F_{is}) were determined from the intersection of real and imaginary components of individual patches (magenta circles, see Results). Additionally, intersections of real and imaginary components for the plotted averaged NLC traces are denoted in the plots by a green

marker. Means and standard errors of the mean (SEM) are reported in figures and legends. T-tests were made in Excel. Methods have been approved by Yale's animal use committee.

S396E knock-in mouse

The S396E knock-in (KI) mouse was generated in D. Oliver's lab, and details are in preparation (Oliver et al., in prep). Briefly, the mPrestin-S396E mice were generated by CRISPR/Cas technology. Cas9 and guide RNA were delivered as RNPs along with a single-stranded DNA (ssDNA) repair template into mouse zygotes by pronuclear injection. The injected zygotes were cultured and allowed to develop to the 2-cell stage before being transferred into recipient C57Bl/6N females. Successful and selective introduction of the single point mutation was verified by sequencing the entire SLC26A5 gene. Mice were backcrossed for > 3 generations to C57Bl/6 mice.

Molecular Dynamics Simulations

Model preparation: Instead of simulating mouse prestin we performed simulations with the closely related structure from gerbil. The simulation model of prestin was built based on the gerbil prestin structure (PDB: 7SUN) and the Alphafold2 gerbil prestin structure (Q9JKQ2 · S26A5_MERUN). The unresolved gap in the structure at residues 159-164 was filled with the corresponding residues in the Alphafold structure after the two models had been superimposed at residues 138-158 and 165-194. The resulting model of wildtype (WT) gerbil prestin was set up in a phosphatidylcholine (POPC) and cholesterol bilayer with a 9:1 ratio and surrounding solvent with a NaCl concentration of 150 mM using the CHARMM-GUI V1.7 web interface (Jo et al., 2008; Lee et al., 2016). In a similar fashion, a model of the S398E mutant was created by using the "mutate residue" functionality in CHARMM-GUI. Both models were then prepared for MD simulation in the same manner as described next. We employed the CHARMM27 force field with cmap for proteins (MacKerell et al., 2004), CHARMM36 for lipids (Klauda et al., 2010) and the CHARMM TIP3P water model. All titratable residues were simulated in their default protonation states at pH7, as predicted by PROPKA 3.1 (Olsson et al., 2011). Relaxation and equilibration were performed following the CHARMM-GUI protocol (Jo et al., 2008) with an initial energy minimization stage and six stages of equilibration during which harmonic restraints on protein and lipids were successively reduced to zero. Simulations were performed at 296 K.

All-atom, explicit solvent Anton MD simulations: Production runs were performed on the Anton 2 supercomputer, a special-purpose computer for molecular MD simulations of biomolecules (Shaw et al., 2014). The system's charge was neutralized with the addition of sodium and chloride ions. Additional sodium and chloride ions were added to produce a free NaCl concentration of 150 mM in solution. The CHARMM36 (MacKerell et al., 1998; MacKerell et al., 2004; Best et al., 2012) force field was used for proteins and ions, and the TIP3P model was used for waters. The RESPA algorithm (Tuckerman et al., 1992) was used to integrate the long-range nonbonded forces every 7.5 fs and short-range nonbonded and bonded forces every 2.5 fs. Long-range electrostatic forces were calculated using the k-Gaussian split Ewald method (Shan et al., 2005). The lengths of bonds to hydrogen atoms were held fixed using the nSHAKE algorithm. The simulations were run at 296K and 1 atm using the Nosé-Hoover chain thermostat (Martyna et al., 1992) and the Martyna-Tobias-Klein (Martyna et al., 1994) barostat, respectively. The RESPA algorithm and temperature and pressure controls were implemented using the multigrator scheme (Lippert et al., 2013) with a time step of 2.5 fs. Temperatures were maintained using Nosé-Hoover chains with time constants τ_T = 0.042 s. Semi-isotropic pressure coupling using Nosé-Hoover chains kept the system at 1 atm across both temperature groups with time constants τ_P = 0.042 s. Coordinates were written to trajectory files every 240 ps.

Simulations were either carried out under equilibrium conditions (0 mV membrane potential) or set up to model a strong negatively polarized membrane of about –150 mV by using the constant electric field approximation (Roux, 2008). A static external electric field in the z direction (a 3-vector electric field [0, 0, -0.024] in unit kcal/mol/Å/e which is an equivalent of -0.00104 V/Å) was applied to the system. Under the constant electric field approximation, the potential drop across the membrane equals the average length of the simulation cell in field direction (145 Å) times the field strength, resulting in approximately –150 mV. In order to avoid sudden changes to the system, the electric field was linearly increased from zero to its maximum value over the initial 200 ns of the simulation; after 200 ns the electric field remained constant for the rest of the simulation.

Anton2 enables the simulation of relatively long times, so here we report 5 µs of trajectory data for WT (at 0 mV and –150 mV) and 2.5 µs for S398E (at 0 mV and –150 mV).

Analysis: Trajectory analysis was carried out with Python scripts based on MDAnalysis (Michaud-Agrawal et al., 2011; Gowers et al., 2016). The radial distribution function (RDF) of Cl^- was calculated for heavy atoms (C, N, O) using the MDAnalysis tool *interRDF*. The RDFs showed that the first shell of ligand atoms of Cl^- in the binding site always lies within a 5 Å radius. Therefore, binding of Cl^- ions to the prestin binding

site was assessed with the following distance criterion: any Cl^- ion within 5 Å of any heavy atoms (carbon, nitrogen, oxygen) of residue 137, 396, 397, 398 was considered bound. Molecular images were prepared in VMD 1.9.3 (Humphrey et al., 1996) and UCSF Chimera (Pettersen et al., 2004).

Results

Figure 1 A and B show the frequency responses of control mouse cNLC in membrane patches. The response is like that of guinea pig prestin in that real and imaginary components of cNLC display differing frequency response, but similar bell-shaped voltage dependence. The absolute magnitude of cNLC, $\sqrt{Re(cNLC)^2 + Im(cNLC)^2}$, near V_h (**Fig. 1B**), displays a stretched-exponential roll-off typical of many physical materials, including viscoelastic behavior of glasses (Langer, 2012), cytoskeleton (Lieleg et al., 2011) and others that must overcome a multitude of energy barriers. For prestin, it indicates that sensor charge movement works against viscoelastic loads within the membrane whose influence is frequency dependent. The average cut-off frequency (F_{is}) is 27.34 +/- 4.31 kHz for the mouse, indicated by the intersection of real and imaginary components, which in a simple 2-state voltage-only Boltzmann model identifies the -3 dB point of absolute cNLC (see Appendix in (Santos-Sacchi and Tan, 2022)). Being stretched-exponential in form, not 2-state Lorentzian, the actual corresponding reduction in Abs(cNLC) at F_{is} is near 90% of half-magnitude. We previously found guinea pig patch F_{is} to be about 19 kHz (Santos-Sacchi et al., 2023), so mouse prestin kinetics appear faster than guinea pig kinetics.

To evaluate cholesterol influence on prestin frequency response, we treated membrane patches with MβCD, a water-soluble compound known to remove membrane cholesterol (Irie et al., 1988; Ilangumaran and Hoessli, 1998). Under whole cell recording conditions, it was previously shown that NLC shifts rightward and peak NLC decreases over exposure time during treatment with MβCD (Rajagopalan et al., 2007; Sfondouris et al., 2008). An example is illustrated in **Fig. 2** where a control (b6) mouse OHC evidences the shift and reduction in NLC over time. A huge positive, depolarizing shift is observed which eventually asymptotes (**Fig. 2B**). Membrane patches, however, do not show these effects, even after >10 minutes of recording (**Fig. 3 A and B**); notably, compared to control, V_h in such patches shows an absence of positive shifts. Indeed the shift is in the negative direction but not statistically significant (-99.5 +/- 7.5 mV vs. -114 +/- 5.6 mV; t-test, 1-tail: p=0.078). Despite an absence of typical whole cell effects of MβCD on membrane patches, prestin kinetics are altered. Since an enhancement in frequency response accompanies increases in plasma membrane fluidity by chloroform treatment (Santos-Sacchi and Tan, 2022), we hypothesized that a similar increase could occur upon removal of membrane cholesterol.

Indeed, compared to control, average F_{is} (**Fig. 3 B**) is increased about 12 kHz (27.34 +/- 4.31 kHz vs. 39.16 +/- 2.94 kHz; t-test, 1-tail: p=0.026).

The influence of membrane lipids on prestin is conjectured to occur at the interface of protein and surrounding lipid bilayer. We and others (Bavi et al., 2021; Ge et al., 2021; Dehghani-Ghahnaviyeh et al., 2022) (Kuwabara et al., 2023) have used molecular dynamics (MD) to investigate such interactions that may reveal conformational states which alter the occupying surface area of prestin, thereby working against the bilayer. Interestingly, we find that interfacial dynamics are not the only mechanism for lipids to interact with prestin. For example, **Fig. 4** illustrates direct insertion of phospholipids into protein crevices created following voltage perturbation. Here we monitor the distance between the center of masses (CoM) of TM 6 (residues 280-282) and TM 12 (residues 462-464) at their cytoplasmic surface. Following delivery of -150 mV to the membrane, over the course of several microseconds, the distance between the CoM's (Δ**D**) increases up to 5.71 Å. During the trajectory time, phospholipids are observed to move and insert into a funnel-like crevice (see supplemental movie 1). These newly rearranged lipids may alter the viscoelastic environment which sensor charges must traverse, possibly accounting for changes in phase of charge movements across frequency that we identify with our cNLC measures (**Fig. 1**).

We previously showed that chloride anions and salicylate can alter prestin kinetics (Santos-Sacchi and Song, 2016; Santos-Sacchi and Tan, 2019). Chloride binding to the identified binding pocket in prestin is not required for the generation of NLC since negatively charged mutations of coordinating residues in the pocket (e.g., residues 396, 398 and 399) can substitute for chloride (Gorbunov et al., 2014; Gorbunov et al., 2018; Butan et al., 2022). Anions have no influence on NLC in that case, presumably because they are not bound. **Fig. 5** shows the results of MD simulations of one such gerbil prestin mutation, S398E, which abrogates anion binding (Butan et al., 2022). In the normal binding pocket, the chloride anion readily interacts with the coordinating residues, whereas with the mutation binding is absent or systematically reduced. What effect does a mutation that removes chloride binding have on cNLC frequency response? We use a KI mouse where the mutation S396E has been engineered into mouse prestin to evaluate this question. **Fig. 6** shows that high frequency charge movements in control and S396E mice OHCs are the same (27.34 +/- 4.31 kHz vs. 29.72 +/-1.67 kHz; t-test, 1-tail: p=0.312). The maintained stretched-exponential behavior in S396E mouse OHCs indicates that the viscoelastic membrane environment dominates the behavior of prestin kinetics at high frequencies. Under whole-cell conditions, altering intracellular chloride results in shifts in V_h (Rybalchenko and Santos-Sacchi, 2003b; Santos-Sacchi et al., 2006b; Rybalchenko and Santos-Sacchi, 2008), increases causing a negative shift. Because the S396E

mutation effectively saturates the chloride binding site, compared to our controls we might expect a V_h shift to negative values. Indeed, a negative shift in V_h relative to controls did occur (-99.5 +/- 7.5 mV vs. -127.8 +/- 7.0 mV; t-test, 1-tail: p=0.017).

Discussion

Prestin works mechanically into the ultrasonic range to enhance our ability to perceive sound through a process termed "cochlear amplification". The kinetics of prestin underlie its ability to influence cochlear mechanics at these high frequencies (Santos-Sacchi and Tan, 2018; Santos-Sacchi, 2019). Beyond intramolecular constraints within prestin itself, the frequency responsiveness of prestin depends on the impinging loads within the membrane bilayer, as well as other cellular/environmental loads (Santos-Sacchi et al., 2019). We previously showed that possible loads associated with the macro-patch technique and membrane tension have little effect on NLC frequency response (Santos-Sacchi and Tan, 2022), so our results here reflect characteristic performance of prestin in the mouse induced by experimental perturbations directly to prestin or the lipid bilayer.

We find that prestin frequency response in normal mice surpasses that we previously measured in the guinea pig (Santos-Sacchi et al., 2023). Mouse NLC cut-off frequency, characterized by F_{is}, where real and imaginary components of cNLC intersect, is about 8 kHz greater than in guinea pig (27 vs. 19 kHz). Considering that the frequency roll-off in prestin is stretched exponential in nature rather than Lorentzian, F_{is} corresponds to a frequency where there is greater than half magnitude reduction in total charge movement, both in and out of phase with voltage, quantified by Abs(cNLC). Consequently, based on the HN fit for the control b6 mouse (**Fig. 1 B**), Abs(cNLC) is down at 80 kHz by 14.73 dB. For the guinea pig we previously found greater roll-off, Abs(cNLC) being down at 80 kHz by 17.71 (Santos-Sacchi et al., 2023).

Chloride binding and NLC

Chloride anions can affect prestin kinetics (Santos-Sacchi and Song, 2016; Santos-Sacchi and Tan, 2022), with mutations altering binding site anion access being influential (Takahashi et al., 2016; Takahashi et al., 2023). Although it had been speculated that Cl^- acts as an extrinsic voltage sensor (Oliver et al., 2001), instead anions likely foster allosteric-like modulation of prestin activity and kinetics (Rybalchenko and Santos-Sacchi, 2003a; Rybalchenko and Santos-Sacchi, 2003b, 2008; Song and Santos-Sacchi, 2010, 2013; Santos-Sacchi and Song, 2016). Binding pocket mutations are confirmatory (e.g., residues 396, 398,

and 399), since they enable voltage dependency of prestin without anion presence (Gorbunov et al., 2014; Gorbunov et al., 2018; Butan et al., 2022). Our MD simulations confirm that the S398E mutation of gerbil prestin halts chloride entry and residence within the anion binding pocket (**Fig. 5**).

Our frequency response measures of S396E NLC indicate no influence of the mutation, F_{is} being no different than that of controls (see above). Based on the HN fit for the S396E mouse, Abs(cNLC) is down at 80 kHz by 14.56 dB. This is essentially the same as the b6 control results. However, we find that the S396E mutation appears to alter V_h in a predictable manner. As we mentioned above, under whole-cell conditions, reducing intracellular chloride results in reversible positive shifts in V_h (Rybalchenko and Santos-Sacchi, 2003b; Santos-Sacchi et al., 2006b; Rybalchenko and Santos-Sacchi, 2008). Given that the S396E mutation essentially saturates the chloride binding site, a significant V_h shift to negative values arises compared to our controls. This negative shift was also found in S396E prestin transfected cells [see supplement in (Takahashi et al., 2023)].

Lipid Bilayer and NLC

While the influence of MβCD on OHC NLC is well documented (Rajagopalan et al., 2007; Sfondouris et al., 2008) and illustrated in **Fig. 2**, showing huge depolarizing shifts in V_h and decreases in peak NLC, these effects are not apparent in membrane patches. Instead, after >10 minutes of exposure to MβCD (0.1 – 1 mM) in the pipette solution, V_h is indistinguishable from control b6 patches, which argues against any induced tension, which normally would shift V_h. In fact, V_h remains sensitive to direct application of tension in MβCD-treated membrane patches (data not shown). Interestingly, this may conflict with previous reports which suggest that MβCD increases membrane tension that acts on stretch channels (Biswas et al., 2019; Cox et al., 2021). It should be noted that while membrane tension itself causes V_h shifts and reductions in peak NLC in whole cell recording mode, in membrane patches there is no reduction in peak NLC during application of membrane tension (Gale and Ashmore, 1997a; Santos-Sacchi and Tan, 2020), indicating that disparities in whole-cell vs. patch recordings are not unusual.

Consequently, given the possible disparities between MβCD effects in whole-cell vs. patch recordings, can we be sure that intra-pipette MβCD actually works on the patch membrane? In fact, NLC frequency analysis indicates that indeed MβCD works on the patch membrane, having effects similar to chloroform treatment (Santos-Sacchi and Tan, 2022). That is, inspection of the frequency response in MβCD-treated patches shows a substantial enhancement, with F_{is} being about 12 kHz greater than control

b6 patch F_{is}. Based on the HN fit for the MβCD-treated patch, Abs(cNLC) is down at 80 kHz by 12.96 dB. This is substantially less roll-off than controls (see above).

Both experimentally and in simulations, the influence of the lipid bilayer has been envisioned to work at its interface with the protein prestin (Santos-Sacchi et al., 1998; Fang et al., 2010; Zhai et al., 2020; Dehghani-Ghahnaviyeh et al., 2022). Interestingly, such interfacial interactions may not be the only mechanism of action. Our MD simulations illustrate that bilayer phospholipids may enter funnels created between transmembrane helices. We speculate that both interfacial interactions and intra-protein interactions may alter the path followed by voltage sensor charge during stimulation. Possibly, the phase of moving charge components will be altered by such deformity of prestin's viscoelastic environment, resulting in the trade-off between real and imaginary components of cNLC across frequency that we find. Clearly, the rapidity of phospholipid movements into prestin could work in the kilohertz range, exactly where prestin influences our ability to hear.

Finally, we note that prestin tertiary structures of all species studied to-date are essentially indistinguishable (Bavi et al., 2021; Ge et al., 2021; Butan et al., 2022; Futamata et al., 2022), yet it is obvious that mammals have evolved to utilize a wide range of species-specific auditory frequency bandwidths. We hypothesize that any special auditory requirements of individual species for cochlear amplification have evolved to capitalize on prestin performance by altering, not the protein itself, but the impinging loads on the protein, including those within the membrane and organ of Corti.

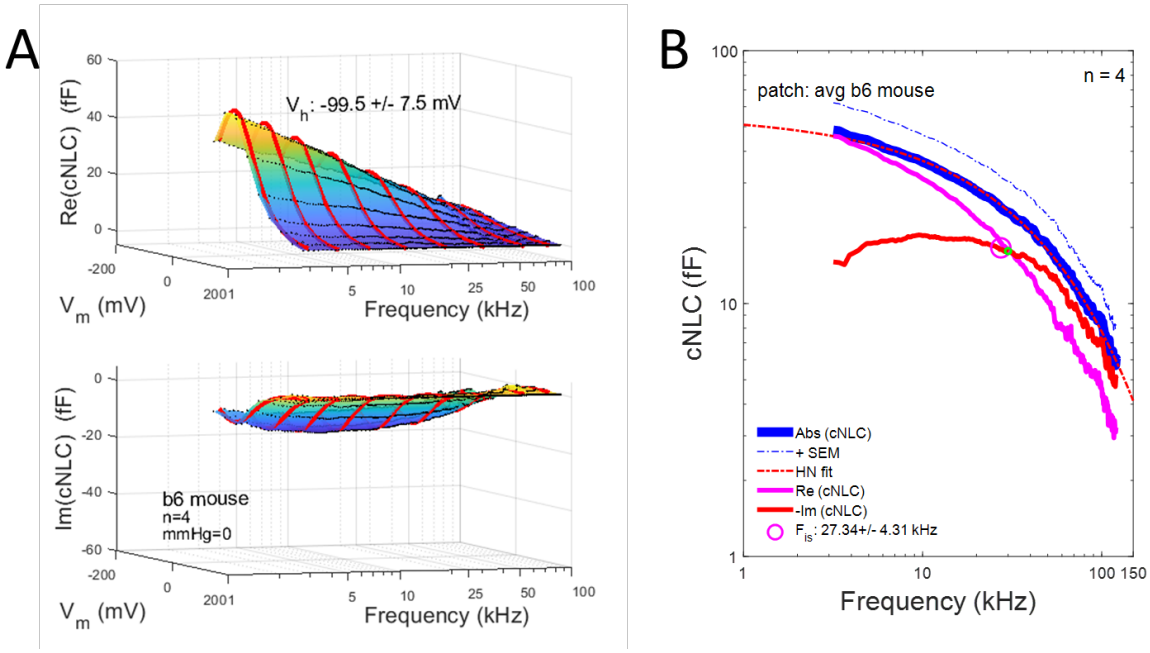

Figure 1. Average complex NLC in control b6 mouse OHC membrane patches. **A)** Real (top panel) and imaginary (bottom panel) components of cNLC across frequency and membrane voltage. Black lines indicate data and red lines are Boltzmann fits at selected frequencies. Average V_h is -99.5 +/- 7.5 mV. Note that real component decreases with frequency while imaginary component increases then decreases with frequency. This pattern is like that of the guinea pig. No pipette pressure is delivered. **B)** Average frequency response of cNLC components near V_h. Abs (cNLC) decreases across frequency in a stretched-exponential manner, indicated by the HN pink dotted line fit. The contribution of the imaginary component to absolute magnitude dominates at the highest frequencies. Average F_{is} (magenta circle) determined from individual recordings is 27.34 +/- 4.31 kHz, faster than that measured in guinea pigs (Santos-Sacchi et al., 2023). Green point marker indicates intersection of averaged traces at 30.0 kHz.

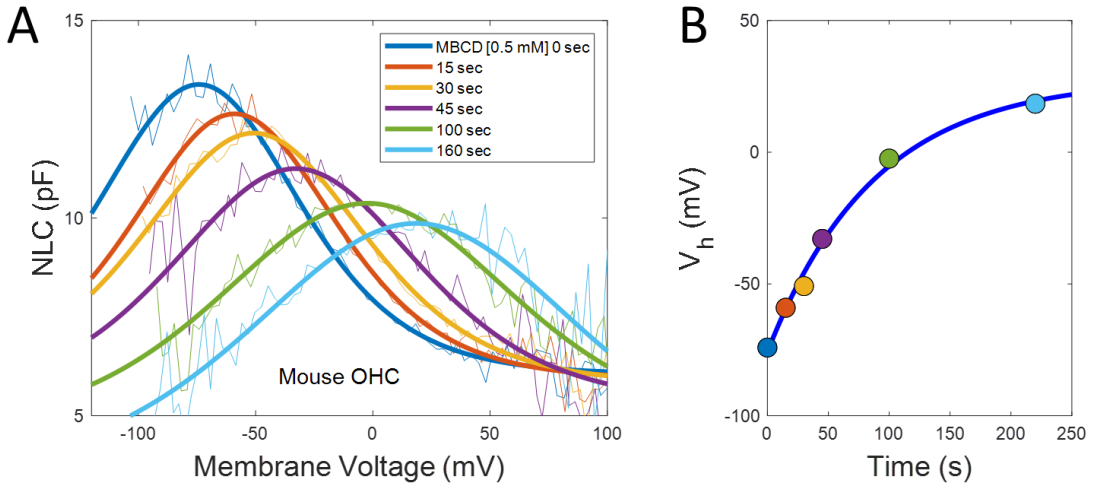

Figure 2. Effect of cholesterol removal by MβCD on whole cell NLC over time. **A)** Bell-shaped NLC shifts rightward and decreases in peak magnitude. NLC was measured with the dual-sine technique. Fitted (*eq.1*) Boltzmann parameters (z, V_h, Q_{max}, C_{lin}) from 0 to 160 seconds exposure are: 0.90, -74.1 mV, 0.84 pC, 6.05 pF; 0.90, -59.0 mV, 0.77 pC, 5.92 pF; 0.81, -50.0 mV, 0.80 pC, 5.8 pF; 0.74, -33.0 mV, 0.83 pC, 5.03 pF; 0.61, 2.4 mV, 0.98 pC, 4.5 pF; 0.55, 18.4 mV, 1.22 pC, 3.3 pF. While V_h estimates are accurately captured at all times, other parameters at later times suffer from reduced voltage range for fitting. **B)** Time course of V_h shift. Within seconds, a huge shift in V_h to depolarizing levels eventually asymptotes.

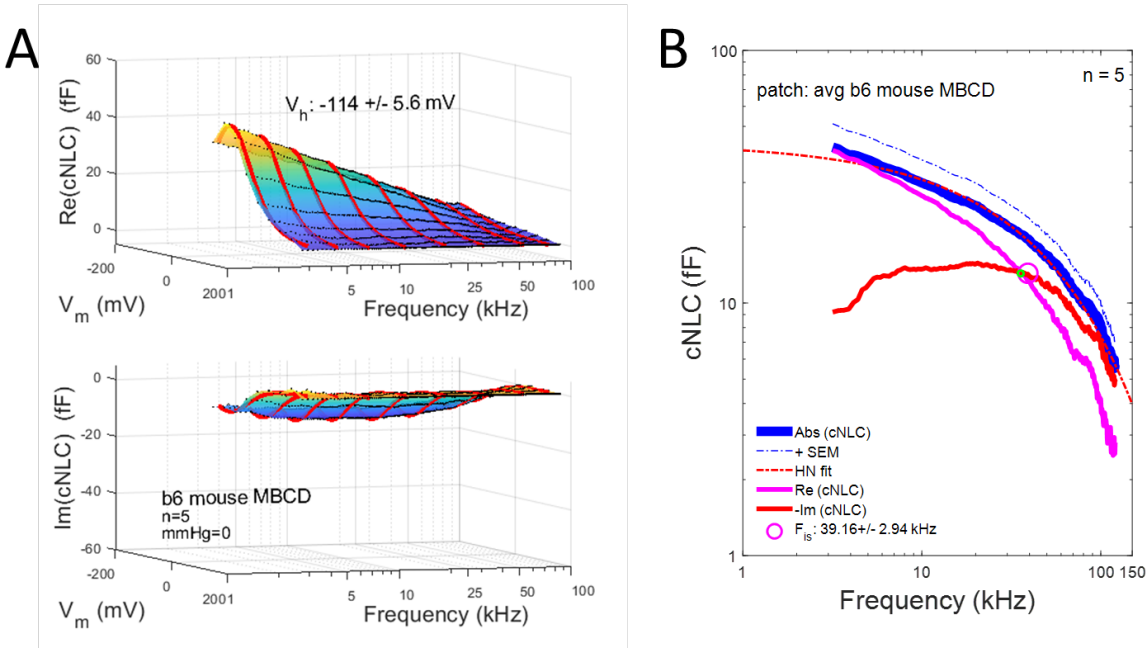

Figure 3. Average complex NLC in b6 mouse OHC membrane patches treated with MβCD. **A)** Real (top panel) and imaginary (bottom panel) components of cNLC across frequency and membrane voltage. Black lines indicate data and red lines are Boltzmann fits at selected frequencies. Average V_h is -114 +/- 5.6 mV. As with controls, real component decreases with frequency while imaginary component increases then decreases with frequency. No pipette pressure is delivered. **B)** Averaged frequency response of cNLC components near V_h. Abs (cNLC) decreases across frequency in a stretched-exponential manner, indicated by the HN pink dotted line fit. Average F_{is} (magenta circle) determined from individual recordings is 39.16 +/- 2.94 kHz, significantly different from controls. Green point marker indicates intersection of averaged traces at 35.7 kHz.

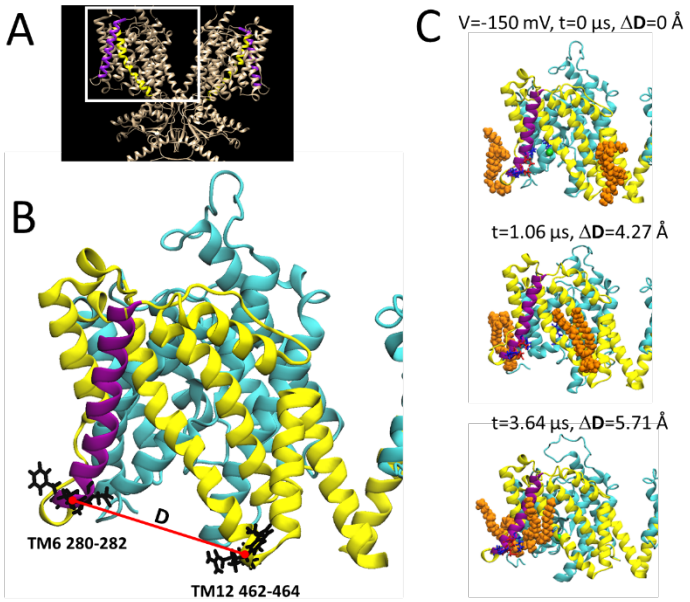

Figure 4. MD simulations show direct insertion of phospholipids into membrane-bound protein crevices created following -150 mV voltage perturbation. **A)** Dimeric structure of gerbil prestin obtained from cryo-EM with TM 6 (purple) and 12 (yellow) highlighted. Boxed in area is displayed in subsequent images. **B)** Red line shows where Δ**D** is monitored between the center of masses (CoM) of TM 6 (residues 280-282) and TM 12 (residues 462-464) at their cytoplasmic surface. Simulations span 5 µs. **C)** Two POPC phospholipids originally external to the transmembrane region of prestin (top panel) move over time into funnel shaped crevice produced by separation of TM 6 and TM 12 (middle and bottom panels).

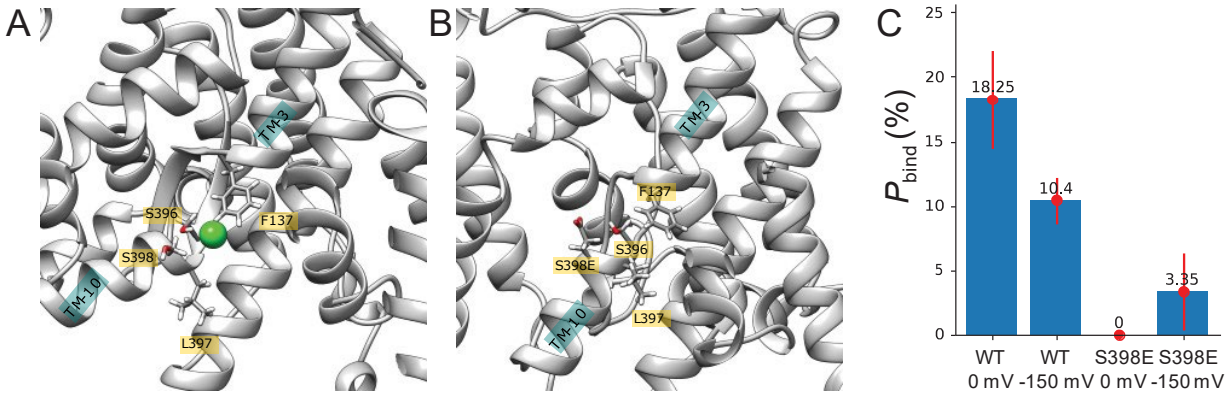

Figure 5. MD simulations show absence of binding in gerbil prestin with mutation S398E. **A)** Snapshot of the anion binding site of WT prestin with bound Cl^- ion (green) between helices TM-3 and TM-10 and residues F132, S396, L397, S398 highlighted. **B)** No stable Cl^- binding was observed in the S398E mutant, which places a negative charge into to the anion binding site. **C)** Binding probability for Cl^- for WT and S398E at 0 mV and –150 mV, reported as an average over the independent binding probabilities observed for protomer A and B. The full error bar represents the absolute value of the difference between the A and B value and is an approximate measure of the variability of obtaining the binding probability from the MD simulations.

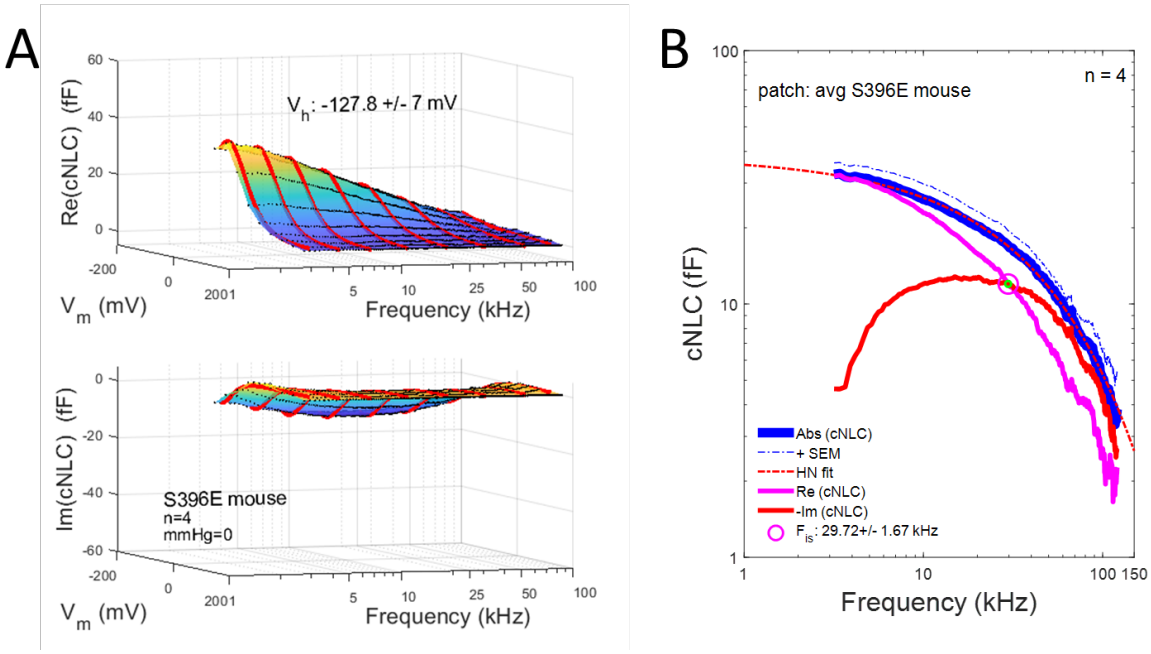

Figure 6. Average complex NLC in S396E mouse OHC membrane patches. **A)** Real (top panel) and imaginary (bottom panel) components of cNLC across frequency and membrane voltage. Black lines indicate data and red lines are Boltzmann fits at selected frequencies. Average V_h is -127.8+/- 7 mV, significantly left-shifted compared to b6 mouse control OHCs. Note that real component decreases with frequency while imaginary component increases then decreases with frequency. No pipette pressure is delivered. **B)** Average frequency response of cNLC components near V_h. Abs (cNLC) decreases across frequency in a stretched-exponential manner, indicated by the HN pink dotted line fit. The contribution of the imaginary component to absolute magnitude dominates at the highest frequencies. Average F_{is} (magenta circle) determined from individual recordings is 29.72 +/- 1.67 kHz, not different from control b6 mouse OHCs. Green point marker indicates intersection of averaged traces at 29.7 kHz.

References

Alverez F, Alegria A, Colmenero J (1991) Relationship between the time-domain Kohlrausch-Williams-Watts and frequency-domain Havriliak-Negami relaxation functions. Physical Review B 44:7306-7312.

Bavi N, Clark MD, Contreras GF, Shen R, Reddy BG, Milewski W, Perozo E (2021) The conformational cycle of prestin underlies outer-hair cell electromotility. Nature 600:553-558.

Best RB, Zhu X, Shim J, Lopes PEM, Mittal J, Feig M, Mackerell J, Alexander D (2012) Optimization of the additive CHARMM all-atom protein force field targeting improved sampling of the backbone ϕ, ψ and side-chain χ_1 and χ_2 dihedral angles. J Chem Theory Comput 8:3257-3273.

Biswas A, Kashyap P, Datta S, Sengupta T, Sinha B (2019) Cholesterol Depletion by MbetaCD Enhances Cell Membrane Tension and Its Variations-Reducing Integrity. Biophys J 116:1456-1468.

Brownell WE, Bader CR, Bertrand D, de Ribaupierre Y (1985) Evoked mechanical responses of isolated cochlear outer hair cells. Science 227:194-196.

Butan C, Song Q, Bai J-P, Tan WJT, Navaratnam D, Santos-Sacchi J (2022) Single particle cryo-EM structure of the outer hair cell motor protein prestin. Nat Commun 13:290.

Cox CD, Zhang Y, Zhou Z, Walz T, Martinac B (2021) Cyclodextrins increase membrane tension and are universal activators of mechanosensitive channels. Proc Natl Acad Sci U S A 118.

Dallos P, Santos-Sacchi J, Flock A (1982) Intracellular recordings from cochlear outer hair cells. Science 218:582-584.

Dallos P, Wu X, Cheatham MA, Gao J, Zheng J, Anderson CT, Jia S, Wang X, Cheng WH, Sengupta S, He DZ, Zuo J (2008) Prestin-based outer hair cell motility is necessary for mammalian cochlear amplification. Neuron 58:333-339.

Dehghani-Ghahnaviyeh S, Zhao Z, Tajkhorshid E (2022) Lipid-mediated prestin organization in outer hair cell membranes and its implications in sound amplification. Nat Commun 13:6877.

Dong X, Ehrenstein D, Iwasa KH (2000) Fluctuation of motor charge in the lateral membrane of the cochlear outer hair cell. Biophys J 79:1876-1882.

Fang J, Izumi C, Iwasa KH (2010) Sensitivity of prestin-based membrane motor to membrane thickness. Biophys J 98:2831-2838.

Fernandez JM, Bezanilla F, Taylor RE (1982) Distribution and kinetics of membrane dielectric polarization. II. Frequency domain studies of gating currents. JGenPhysiol 79:41-67.

Futamata H, Fukuda M, Umeda R, Yamashita K, Tomita A, Takahashi S, Shikakura T, Hayashi S, Kusakizako T, Nishizawa T, Homma K, Nureki O (2022) Cryo-EM structures of thermostabilized prestin provide mechanistic insights underlying outer hair cell electromotility. Nat Commun 13:6208.

Gale JE, Ashmore JF (1994) Charge displacement induced by rapid stretch in the basolateral membrane of the guinea-pig outer hair cell. Proc R Soc Lond B Biol Sci 255:243-249.

Gale JE, Ashmore JF (1997a) The outer hair cell motor in membrane patches. Pflugers Arch 434:267-271.

Gale JE, Ashmore JF (1997b) An intrinsic frequency limit to the cochlear amplifier. Nature 389:63-66.

Ge J, Elferich J, Dehghani-Ghahnaviyeh S, Zhao Z, Meadows M, von Gersdorff H, Tajkhorshid E, Gouaux E (2021) Molecular mechanism of prestin electromotive signal amplification. Cell 184:4669-4679 e4613.

Geertsma ER, Oliver D (2023) SLC26 Anion Transporters. Handb Exp Pharmacol.

Gorbunov D, Hartmann J, Renigunta V, Oliver D (2018) A glutamate scan identifies an electrostatic switch for prestin activity. Midwinter Meeting Abstracts of the Associatio for Research in Otolaryngology.

Gorbunov D, Sturlese M, Nies F, Kluge M, Bellanda M, Battistutta R, Oliver D (2014) Molecular architecture and the structural basis for anion interaction in prestin and SLC26 transporters. Nat Commun 5:3622.

Gowers RJ, Linke M, Barnoud J, Reddy TJE, Melo MN, Seyler SL, Dotson DL, Domański J, Buchoux S, Kenney IM, Beckstein O (2016) MDAnalysis: A Python package for the Rapid Analysis of Molecular Dynamics Simulations. In: Proceedings of the 15th Python in Science Conference (Benthall S, Rostrup S, eds), pp 98--105. Austin, TX.

Humphrey W, Dalke A, Schulten K (1996) VMD -- Visual Molecular Dynamics. J Molecular Modelling 14:33--38.

Ilangumaran S, Hoessli DC (1998) Effects of cholesterol depletion by cyclodextrin on the sphingolipid microdomains of the plasma membrane. Biochem J 335 (Pt 2):433-440.

Irie T, Fukunaga K, Yoshida A, Uekama K, Fales HM, Pitha J (1988) Amorphous water-soluble cyclodextrin derivatives: 2-hydroxyethyl, 3-hydroxypropyl, 2-hydroxyisobutyl, and carboxamidomethyl derivatives of beta-cyclodextrin. Pharm Res 5:713-717.

Iwasa KH (1993) Effect of stress on the membrane capacitance of the auditory outer hair cell. Biophys J 65:492-498.

Jo S, Kim T, Iyer VG, Im W (2008) CHARMM-GUI: a web-based graphical user interface for CHARMM. J Comput Chem 29:1859-1865.

Kakehata S, Santos-Sacchi J (1995) Membrane tension directly shifts voltage dependence of outer hair cell motility and associated gating charge. Biophys J 68:2190-2197.

Kamar RI, Organ-Darling LE, Raphael RM (2012) Membrane cholesterol strongly influences confined diffusion of prestin. Biophys J 103:1627-1636.

Klauda JB, Venable RM, Freites JA, O'Connor JW, Tobias DJ, Mondragon-Ramirez C, Vorobyov I, MacKerell J, Alexander D, Pastor RW (2010) Update of the CHARMM all-atom additive force field for lipids: validation on six lipid types. J Phys Chem B 114:7830-7843.

Kuwabara MF, Haddad BG, Lenz-Schwab D, Hartmann J, Longo P, Huckschlag BM, Fuss A, Questino A, Berger TK, Machtens JP, Oliver D (2023) Elevator-like movements of prestin mediate outer hair cell electromotility. Nat Commun 14:7145.

Langer JS (2012) Shear-transformation-zone theory of viscosity, diffusion, and stretched exponential relaxation in amorphous solids. Phys Rev E Stat Nonlin Soft Matter Phys 85:051507.

Lee J, Cheng X, Swails JM, Yeom MS, Eastman PK, Lemkul JA, Wei S, Buckner J, Jeong JC, Qi Y, Jo S, Pande VS, Case DA, Brooks r, Charles L, MacKerell J, Alexander D, Klauda JB, Im W (2016) CHARMM-GUI Input Generator for NAMD, GROMACS, AMBER, OpenMM, and CHARMM/OpenMM Simulations Using the CHARMM36 Additive Force Field. J Chem Theory Comput 12:405-413.

Lieleg O, Kayser J, Brambilla G, Cipelletti L, Bausch AR (2011) Slow dynamics and internal stress relaxation in bundled cytoskeletal networks. Nat Mater 10:236-242.

Lippert RA, Predescu C, Ierardi DJ, Mackenzie KM, Eastwood MP, Dror RO, Shaw DE (2013) Accurate and efficient integration for molecular dynamics simulations at constant temperature and pressure. J Chem Phys 139:164106.

MacKerell A et al. (1998) All-atom empirical potential for molecular modeling and dynamics studies of proteins. JPhysChemB 102:3586--3616.

MacKerell J, A. D., Feig M, Brooks III CL (2004) Extending the treatment of backbone energetics in protein force fields: limitations of gas-phase quantum mechanics in reproducing protein conformational distributions in molecular dynamics simulations. JCompChem 25:1400--1415.

Martyna GJ, Klein ML, Tuckerman M (1992) Nosé–Hoover chains: The canonical ensemble via continuous dynamics. The Journal of Chemical Physics 97:2635-2643.

Martyna GJ, Tobias DJ, Klein ML (1994) Constant pressure molecular dynamics algorithms. J Chem Phys 101:4177-4189.

Mason MJ, Simpson AK, Mahaut-Smith MP, Robinson HP (2005) The interpretation of current-clamp recordings in the cell-attached patch-clamp configuration. Biophys J 88:739-750.

Michaud-Agrawal N, Denning EJ, Woolf TB, Beckstein O (2011) MDAnalysis: A Toolkit for the Analysis of Molecular Dynamics Simulations. J Comp Chem 32:2319--2327.

Oliver D, He DZ, Klocker N, Ludwig J, Schulte U, Waldegger S, Ruppersberg JP, Dallos P, Fakler B (2001) Intracellular anions as the voltage sensor of prestin, the outer hair cell motor protein. Science 292:2340-2343.

Olsson MHM, Søndergaard CR, Rostkowski M, Jensen JH (2011) PROPKA3: Consistent Treatment of Internal and Surface Residues in Empirical $\mathrmpK_\mathrma$ Predictions. J Chem Theory Comput 7:525-537.

Organ LE, Raphael RM (2009) Lipid lateral mobility in cochlear outer hair cells: regional differences and regulation by cholesterol. JAssocResOtolaryngol 10:383-396.

Pettersen EF, Goddard TD, Huang CC, Couch GS, Greenblatt DM, Meng EC, Ferrin TE (2004) UCSF Chimera--a visualization system for exploratory research and analysis. J Comput Chem 25:1605-1612.

Rajagopalan L, Greeson JN, Xia A, Liu H, Sturm A, Raphael RM, Davidson AL, Oghalai JS, Pereira FA, Brownell WE (2007) Tuning of the outer hair cell motor by membrane cholesterol. JBiolChem 282:36659-36670.

Roux B (2008) The membrane potential and its representation by a constant electric field in computer simulations. BiophysJ 95:4205--4216.

Russell IJ, Sellick PM (1978) Intracellular studies of hair cells in the mammalian cochlea. JPhysiol (Lond) 284:261-290.

Rybalchenko V, Santos-Sacchi J (2003a) Allosteric modulation of the outer hair cell motor protein prestin by chloride. In: Biophysics of the Cochlea: From Molecules to Models (Gummer A, ed), pp 116-126. Singapore: World Scientific Publishing.

Rybalchenko V, Santos-Sacchi J (2003b) Cl- flux through a non-selective, stretch-sensitive conductance influences the outer hair cell motor of the guinea-pig. J Physiol 547:873-891.

Rybalchenko V, Santos-Sacchi J (2008) Anion control of voltage sensing by the motor protein prestin in outer hair cells. Biophys J 95:4439-4447.

Santos-Sacchi J (1991) Reversible inhibition of voltage-dependent outer hair cell motility and capacitance. J Neurosci 11:3096-3110.

Santos-Sacchi J (2004) Determination of cell capacitance using the exact empirical solution of dY/dCm and its phase angle. Biophys J 87:714-727.

Santos-Sacchi J (2019) The speed limit of outer hair cell electromechanical activity. HNO 67:159-164.

Santos-Sacchi J, Dilger JP (1988) Whole cell currents and mechanical responses of isolated outer hair cells. Hear Res 35:143-150.

Santos-Sacchi J, Navarrete E (2002) Voltage-dependent changes in specific membrane capacitance caused by prestin, the outer hair cell lateral membrane motor. Pflugers Arch 444:99-106.

Santos-Sacchi J, Wu M (2004) Protein- and lipid-reactive agents alter outer hair cell lateral membrane motor charge movement. JMembrBiol 200:83-92.

Santos-Sacchi J, Song L (2016) Chloride anions regulate kinetics but not voltage-sensor Qmax of the solute carrier SLC26a5. Biophys J 110:1-11.

Santos-Sacchi J, Tan W (2018) The Frequency Response of Outer Hair Cell Voltage-Dependent Motility Is Limited by Kinetics of Prestin. J Neurosci 38:5495-5506.

Santos-Sacchi J, Tan W (2019) Voltage Does Not Drive Prestin (SLC26a5) Electro-Mechanical Activity at High Frequencies Where Cochlear Amplification Is Best. iScience 22:392-399.

Santos-Sacchi J, Tan W (2020) Complex nonlinear capacitance in outer hair cell macro-patches: effects of membrane tension. Sci Rep 10:6222.

Santos-Sacchi J, Tan W (2022) On the frequency response of prestin charge movement in membrane patches. Biophys J May 20;S0006-3495(22)00413-1. .

Santos-Sacchi J, Kakehata S, Takahashi S (1998) Effects of membrane potential on the voltage dependence of motility-related charge in outer hair cells of the guinea-pig. J Physiol 510 (Pt 1):225-235.

Santos-Sacchi J, Iwasa KH, Tan W (2019) Outer hair cell electromotility is low-pass filtered relative to the molecular conformational changes that produce nonlinear capacitance. J Gen Physiol 151:1369-1385.

Santos-Sacchi J, Navaratnam D, Tan WJT (2021) State dependent effects on the frequency response of prestin's real and imaginary components of nonlinear capacitance. Sci Rep 11:16149.

Santos-Sacchi J, Bai JP, Navaratnam D (2023) Megahertz Sampling of Prestin (SLC26a5) Voltage-Sensor Charge Movements in Outer Hair Cell Membranes Reveals Ultrasonic Activity that May Support Electromotility and Cochlear Amplification. J Neurosci 43:2460-2468.

Santos-Sacchi J, Song L, Zheng J, Nuttall AL (2006a) Control of mammalian cochlear amplification by chloride anions. J Neurosci 26:3992-3998.

Santos-Sacchi J, Song L, Zheng JF, Nuttall AL (2006b) Control of mammalian cochlear amplification by chloride anions. J Neurosci 26:3992-3998.

Sfondouris J, Rajagopalan L, Pereira FA, Brownell WE (2008) Membrane composition modulates prestin-associated charge movement. JBiolChem 283:22473-22481.

Shan Y, Klepeis JL, Eastwood MP, Dror RO, Shaw DE (2005) Gaussian split Ewald: A fast Ewald mesh method for molecular simulation. J Chem Phys 122:54101.

Shaw DE et al. (2014) Anton 2: Raising the Bar for Performance and Programmability in a Special-Purpose Molecular Dynamics Supercomputer. In: SC '14: Proceedings of the International Conference for High Performance Computing, Networking, Storage and Analysis, pp 41-53.

Song L, Santos-Sacchi J (2010) Conformational state-dependent anion binding in prestin: evidence for allosteric modulation. Biophys J 98:371-376.

Song L, Santos-Sacchi J (2013) Disparities in voltage-sensor charge and electromotility imply slow chloride-driven state transitions in the solute carrier SLC26a5. Proc Natl Acad Sci U S A.

Takahashi S, Santos-Sacchi J (2001) Non-uniform mapping of stress-induced, motility-related charge movement in the outer hair cell plasma membrane. Pflugers Arch 441:506-513.

Takahashi S, Cheatham MA, Zheng J, Homma K (2016) The R130S mutation significantly affects the function of prestin, the outer hair cell motor protein. J Mol Med (Berl) 94:1053-1062.

Takahashi S, Zhou Y, Kojima T, Cheatham MA, Homma K (2023) Prestin's fast motor kinetics is essential for mammalian cochlear amplification. Proc Natl Acad Sci U S A 120:e2217891120.

Tuckerman M, Berne BJ, Martyna GJ (1992) Reversible multiple time scale molecular dynamics. The Journal of Chemical Physics 97:1990-2001.

Zhai F, Song L, Bai JP, Dai C, Navaratnam D, Santos-Sacchi J (2020) Maturation of Voltage-induced Shifts in SLC26a5 (Prestin) Operating Point during Trafficking and Membrane Insertion. Neuroscience 431:128-133.

Zheng J, Shen W, He DZ, Long KB, Madison LD, Dallos P (2000) Prestin is the motor protein of cochlear outer hair cells. Nature 405:149-155.